Research Article | Vol. 25, No. 15 | 24 Jul 2017 | OPTICS EXPRESS 17892
Optics EXPRESS

Single-shot determination of focused FEL wave fields using iterative phase retrieval

MASOUD MEHRJOO,[1,2] KLAUS GIEWEKEMEYER,[2] PATRIK VAGOVIČ,[2,3] STEPHAN STERN,[2,3] RICHARD BEAN,[2] MARC MESSERSCHMIDT,[2,4] BARBARA KEITEL,[3] ELKE PLÖNJES,[3] MARION KUHLMANN,[3] TOBIAS MEY,[5] EVGENY A. SCHNEIDMILLER,[3] MIKHAIL V. YURKOV,[3] TORSTEN LIMBERG,[3] AND ADRIAN P. MANCUSO[2,*]

[1] *University of Hamburg, The Hamburg Centre for Ultrafast Imaging, Luruper Chaussee 149, 22761 Hamburg, Germany*
[2] *European XFEL, Holzkoppel 4, 22869 Schenefeld, Germany*
[3] *Deutsches Elektronen-Synchrotron, Notkestraße 85, 22607 Hamburg, Germany*
[4] *National Science Foundation BioXFEL Science and Technology Center, Buffalo, NY 14203, USA*
[5] *Laser-Laboratorium Göttingen e.V., Hans-Adolf-Krebs-Weg 1, 37077 Göttingen, Germany*
[*] *adrian.mancuso@xfel.eu*

Abstract: Determining fluctuations in focus properties is essential for many experiments at Self-Amplified-Spontaneous-Emission (SASE) based Free-Electron-Lasers (FELs), in particular for imaging single non-crystalline biological particles. We report on a diffractive imaging technique to fully characterize highly focused, single-shot pulses using an iterative phase retrieval algorithm, and benchmark it against an existing Hartmann wavefront sensor. The results, both theoretical and experimental, demonstrate the effectiveness of this technique to provide a comprehensive and convenient shot-to-shot measurement of focused-pulse wave fields and source-point positional variations without the need for manipulative optics between the focus and the detector.

OCIS codes: (140.2600) Free-electron lasers (FELs); (340.7440) X-ray imaging; (340.0340) X-ray optics.

References and links

1. A. Altarelli, "The European X-ray free-electron laser facility in Hamburg," Nucl. Instrum. Methods Phys. Res. B **269**, 2845–2849 (2011).
2. P. Emma, R. Akre, J. Arthur, R. Bionta, C. Bostedt, J. Bozek, A. Brachmann, P. Bucksbaum, R. Coffee, F. J. Decker, Y. Ding, D. Dowell, S. Edstrom, A. Fisher, J. Frisch, S. Gilevich, J. Hastings, G. Hays, Ph. Hering, Z. Huang, R. Iverson, H. Loos, M. Messerschmidt, A. Miahnahri, S. Moeller, H. D. Nuhn, G. Pile, D. Ratner, J. Rzepiela, D. Schultz, T. Smith, P. Stefan, H. Tompkins, J. Turner, J. Welch, W. White, J. Wu, G. Yocky, and J. Galayda, "First lasing and operation of an *Å*ngstrom-wavelength free-electron laser," Nat. Photonics **4**, 641–647 (2010).
3. T. Ishikawa, H. Aoyagi, T. Asaka, Y. Asano, N. Azumi, T. Bizen, H. Ego, K. Fukami, T. Fukui, Y. Furukawa, S. Goto, H. Hanaki, T. Hara, T. Hasegawa, T. Hatsui, A. Higashiya, T. Hirono, N. Hosoda, M. Ishii,T. Inagaki, Y. Inubushi, T. Itoga, Y. Joti, M. Kago, T. Kameshima, H. Kimura, Y. Kirihara, A. Kiyomichi, T. Kobayashi, C. Kondo, T. Kudo, H. Maesaka, X. M. Maréchal, T. Masuda, S. Matsubara, T. Matsumoto, T. Matsushita, S. Matsui, M. Nagasono, N. Nariyama, H. Ohashi, T. Ohata, T. Ohshima, S. Ono, Y. Otake, C. Saji, T. Sakurai, T. Sato, K. Sawada, T. Seike, K. Shirasawa, T. Sugimoto, S. Suzuki, S. Takahashi, H. Takebe, K. Takeshita, K. Tamasaku, H. Tanaka, R. Tanaka, T. Tanaka, T. Togashi, K. Togawa, A. Tokuhisa, H. Tomizawa, K. Tono, S. Wu, M. Yabashi, M. Yamaga, A. Yamashita, K. Yanagida, C. Zhang, T. Shintake, H. Kitamura, and N. Kumagai, "A compact X-ray free-electron laser emitting in the sub-*Å*ngström region," Nat. Photonics **6**, 540–544 (2012).
4. H. N. Chapman, A. Barty, M. J. Bogan, S. Boutet, M. Frank, S. P. Hau-Riege, S. Marchesini, B. W. Woods, S. C. Bajt, W. H. Benner, R. A. London, E. Plönjes, M. Kuhlmann, R. Treusch, S. Dösterer, T. Tschentscher, J. R. Schneider, E. Spiller, T. Möller, C. Bostedt, M. Hoener, D. A. Shapiro, K. O. Hodgson, D. van der Spoel, F. Burmeister, M. Bergh, C. Caleman, G. Huldt, M. M. Seibert, F. R. N. C. Maia, R. W. Lee, A. Szöke, N. Timneanu, and J. Hajdu, "Femtosecond diffractive imaging with a soft-X-ray free-electron laser," Nat. Phys. **2**, 839–843 (2006).
5. A. Barty, S. Boutet, M. J. Bogan, S. Hau-Riege, S. Marchesini, K. Sokolowski-Tinten, N. Stojanovic, R. Tobey, H. Ehrke, A. Cavalleri, S. Düsterer, M. Frank, S. C. Bajt, B. W. Woods, M. M. Seibert, J. Hajdu, R. Treusch, and H. N. Chapman, "Ultrafast single-shot diffraction imaging of nanoscale dynamics," Nat. Photon. **2**, 415–419 (2008).
6. A. Barty, J. Küpper, and H. N. Chapman, "Molecular Imaging Using X-Ray Free-Electron Lasers," Ann. Phys. Rev. Chem. **64**, 415–435 (2013).

#293355 https://doi.org/10.1364/OE.25.017892
Journal © 2017 Received 26 Apr 2017; revised 16 Jun 2017; accepted 18 Jun 2017; published 18 Jul 2017

Optics EXPRESS

7. R. Falcone, M. Dunne, H. N. Chapman, M. Yabashi, and K. Ueda, "Frontiers of free-electron laser science II," J. Phys. B **49**, 180201 (2016).
8. B. W. J. McNeil and N. R. Thompson, "X-ray free-electron lasers," Nat. Photon. **4**, 814–821 (2010).
9. D. Shapiro, P. Thibault, T. Beetz, V. Elser, M. Howells, C. Jacobsen, J. Kirz, E. Lima, H. Miao, A. M. Neiman, and D. Sayre, "Biological imaging by soft x-ray diffraction microscopy," in *Proceedings of the National Academy of Sciences of the United States of America,* M. M. Murnane, ed. (Academic, 2005), 15343–15346.
10. A. Schropp and C. G. Schroer, "Dose requirements for resolving a given feature in an object by coherent x-ray diffraction imaging," New. J. Phys. **12**, 035016 (2010).
11. A. Barty, R. Soufli, T. McCarville, S. L. Baker, M. J. Pivovaroff, P. Stefan, and R. Bionta, "Predicting the coherent X-ray wavefront focal properties at the Linac Coherent Light Source (LCLS) X-ray free electron laser," Opt. Express **17**, 15508–15519 (2009).
12. B. Keitel, E. Plönjes, S. Kreis, M. Kuhlmann, K. Tiedtke, T. May ,B. Schäfe, and K. Mann, "Hartmann wavefront sensors and their application at FLASH," J. Synchrotron Rad. **23**, 43–49 (2016).
13. B. Schäfer, M. Lübbecke, and K. Mann, "Hartmann-Shack wave front measurements for real time determination of laser beam propagation parameters," Rev. Sci. Instrum, **77**, 053103 (2006).
14. P. Mercère, P. Zeitoun, M. Idir, S. Le Pape, D. Douillet, X. Levecq, G. Dovillaire, S. Bucourt, K. A. Goldberg, P. P. Naulleau, and S. Rekawa, "Hartmann wave-front measurement at 13.4 nm with $\frac{\lambda_{EUV}}{120}$ accuracy," Opt. Express **28**,1534–1536 (2003).
15. S. Rutishauser, L. Samoylova, J. Krzywinski, O. Bunk, J. Grünert, H. Sinn, M. Cammarata, D. M. Fritz, and C. David, "Exploring the wavefront of hard X-ray free-electron laser radiation," Nat. Commun. **3**, 947 (2012).
16. A. Schropp, R. Hoppe, V. Meier, J. Patommel, F. Seiboth, H. J. Lee, B. Nagler, E. C. Galtier, B. Arnold, U. Zastrau, J. B. Hastings, D. lNilsson, F. Uhlén, U. Vogt, H. M. Hertz, and C. G. Schroer, "Full spatial characterization of a nanofocused x-ray free-electron laser beam by ptychographic imaging," Sci. Rep. **3**, 1633 (2013).
17. H. H. Barret,C. Dainty, and D. Lara, "Maximum-likelihood methods in wavefront sensing: stochastic models and likelihood functions," J. Opt. Soc. Am. A **24**, 391–414 (2007).
18. R. W. Gerchberg, and W. O. Saxton, "Wave phase from image and diffraction plane pictures," in *Image processing and computer-aided design in electron optics*, P. W. Hawkes, ed. (Academic, 1973).
19. S. Marchesini, H. He, H. N. Chapman, S. P. Hau-Riege, A. Noy, M. R. Howells, U. Weierstall, and J. C. H. Spence, 'X-ray image reconstruction from a diffraction pattern alone," Phys. Rev. B **68**, 140101(R) (2003).
20. V. Elser,"Phase retrieval by iterated projections," J. Opt. Soc. Am. A **20**, 40–55 (2003).
21. H. M. Quiney, A. G. Peele, Z. Cai, D. Paterson, and K. A. Nugent, "Diffractive imaging of highly focused X-ray fields," Nature **2**, 101–104 (2006).
22. G. J. Williams, H. M. Quiney, B . B. Dhal, C. Q. Tran, K. A. Nugent, A. G. Peele, D. Patterson, and M. D. de Jounge, "Fresnel Coherent Diffractive Imaging," Phys. Rev. Lett. **97**, 025506 (2006).
23. G. J. Williams, H. M. Quiney, A . G. Peele, and K. A. Nugent, "Fresnel coherent diffractive imaging: Treatment and analysis of data," New. J. Phys. **12**, 035020 (2010).
24. K. A. Nugent, A. G. Peele, H. M. Quiney, and H. N. Chapman, "Diffraction with wavefront curvature: a path to unique phase recovery," Acta Cryst. **61**, 373–381 (2005).
25. T. A. Pitts, and J. F. Greenleaf, "Fresnel transform phase retrieval from magnitude," IEEE Transactions on Ultrasonics Ferroelectrics and Frequency Control. **50**, 1035–1045 (2005).
26. F. Mastropietro, D. Carbone, A. Diaz, J. Eymery, A. Sentenac, T. H. Metzger, V. Chamard, and V. Favre-Nicolin, "Coherent x-ray wavefront reconstruction of a partially illuminated fresnel zone plate," Opt. Express **19**, 19223–19232 (2011).
27. E. L. Saldin, E. A. Schneidmiller, and M. V. Yurkov, *The physics of free electron lasers*, (Springer, 2000), Chap. 2.
28. K. Tiedtke, A. Azima, N. von Bargen, L. Bittner, S. Bonfigt, S. Düsterer, B. Faatz, U. Frühling, M. Gensch, C. Gerth, N. Guerassimova, U. Hahn, T. Hans, M. Hesse, K. Honkavaar, U. Jastrow, P. Juranic, S. Kapitzki, B. Keitel, T. Kracht, M. Kuhlmann, W. B. Li, M. Martins, T. Nunez, E. Plönjes, H. Redlin, E. L. Saldin, E. A. Schneidmiller, J. R. Schneider, S. Schreiber, N. Stojanovic, F. Tavella, S. Toleikis, R. Treusch, H. Weigelt, M. Wellhöfer, H. Wabnitz, M. V. Yurkov, and J. Feldhaus, "The soft x-ray free-electron laser FLASH at DESY: beamlines, diagnostics and end-stations," New. J. Phys. **11**, 023029 (2009).
29. J. R. Fienup, "Phase retrieval algorithms: a comparison," Appl. Opt. **21**, 2758–2769 (1982).
30. J. R. Fienup, "Phase-retrieval algorithms for a complicated optical system," Appl. Opt. **32**, 1737–1746 (1993).
31. J. W. Goodman, *Introduction to Fourier Optics*, (Roberts and Company Publishers, 2005), Chap. 4.
32. D. M. Paganin, *Coherent X-ray Optics*, (Oxford University, 2006), Chap. 1.
33. D. Sayer, "Some implications of a theorem due to Shannon," Acta Crystallogr. **5**, 843 (1952).
34. O. Levent, "Sampling of the diffraction field," Appl. Opt. **39**, 5929–5935 (2000).
35. J. Vila-Comamala, A. Diaz, M. Guizar-Sicairos, A. Mantion, C. M. Kewish, A. Menzel, O. Bunk, and C. David, "Characterization of high-resolution diffractive X-ray optics by ptychographic coherent diffractive imaging," Opt. Express **19**, 21333–21344 (2011).
36. R. Cusack, and N. Papadakis, "New Robust 3-D Phase Unwrapping Algorithms: Application to Magnetic Field Mapping and Undistorting Echoplanar Images," NeuroImage **16**, 754–764 (2002).
37. P. Emma, "Bunch Compression," in *Handbook of Accelerator Physics and Engineering,* A. W. Chao, K. H. Mess, M. Tinger, F. Zimmermann, eds. (Academic, 2013).

Optics EXPRESS

38. E. A. Schneidmiller and M. V. Yurkov, "Coherence properties of the radiation from FLASH," J. Mod. Opt. , **64**, 293–308 (2016)
39. B. Flöter, *Strahlcharakterisierung von Freie-Elektronen-Lasern im weichen Röntgen-Spektralbereich* , (Göttingen series in x-ray physics, 2012), chap. 3.
40. http://www.imagine-optic.com
41. http://www.llg-ev.de
42. Y. Carmon, and E. N. Ribak, "Fast Fourier demodulation," Appl. Phys. Lett. **84**, 4656 (2004).
43. Y. Carmon, and E. N. Ribak, "Phase retrieval by demodulation of a hartmann-shack sensor," Opt. Commun. **215**, 285–288 (2003).
44. Y. Canvas, and E. N. Ribak, "Comparison of hartmann analysis methods," Appl. Opt. **46**, 1830–1835 (2007).
45. N. Zon, O. Srour, and E. N. Ribak, "Hartmann-shack analysis errors," Opt. Express **14**, 635–643 (2006).
46. M. Mehrjoo, University of Hamburg, The Hamburg Centre for Ultrafast Imaging, Luruper Chaussee 149, 22761 Hamburg, Germany, is preparing a Ph.D. thesis to be called "X-ray beam characterization for single particle imaging experiments at Free-Electron-Lasers (FELs): Optimizing wavefront and source characteristics."

1. Introduction

The advent of hard X-ray Free-Electron-lasers (XFEL), such as the European XFEL [1] in the Hamburg area, Germany, the Linac Coherent Light Source (LCLS) [2], CA, USA or the SPring-8 Angstrom Compact free electron LAser (SACLA) [3], Japan, enables a broad range of novel experiments including single-shot diffraction imaging of biological structures [4] and time-resolved imaging of the dynamics of matter [5]. The unique properties of XFEL radiation; such as femtosecond pulse duration, high peak power and high transverse coherence; pave the way for these novel experiments [6–8]. Many experiments at FELs require a high degree of X-ray beam focusing to obtain the highest intensity or an optimal matching between beam size and the spatial extent of samples to be injected [9, 10]. To enable a complete analysis of data for a large fraction of experiments performed at FELs with focused beams, it is important to know the exact properties of the focused complex wave fields including the phase, intensity and spatial distribution. This is particularly the case for imaging experiments which require either a well-defined or well-characterised wavefield to quantitatively interpret the structure of the sample investigated.

The characterization of highly focused X-ray pulses is particularly challenging due to the stochastic shot-to-shot fluctuations of the SASE process as well as a focused peak intensity that exceeds the damage threshold of any material [11].

Over the last few years, a variety of techniques have been developed to characterize FEL pulses, such as Hartmann Wavefront Sensing (HWS) [12–14], X-ray Grating Interferometry (XGI) [15] and Ptychographic Coherent X-ray Diffractive Imaging (PCDI) [16]. In the former approaches, pinhole arrays or gratings are designed for a limited range of photon energies. The accuracy of reconstructions specifically relies on the assumption of a small-angle deflection, which decreases the sensitivity to small local phase changes [17]. The latter approach requires a large ensemble of measurements, in the presence of a sample, to retrieve the illuminating probe, so that a statistically averaged picture of the focused beam is obtained [10].

A solution to overcome these problems is to use an iterative diffractive imaging technique [18–20] applied to single far-field diffraction patterns of a highly focused beam [21]. This method comprises an Iterative Phase Retrieval Algorithm (IPRA) with real space and intensity modulus constraints, utilizing the spherical phase curvature of the focused beam; known as the Fresnel Coherent Diffraction Imaging (FCDI) method [22, 23]. This modification results in the fast and predominantly reliable convergence of the algorithm [24, 25].

In this work, we propose an extension of the FCDI method to systematically characterize highly focused X-ray pulses under more general experimental conditions than previously assumed [21, 26]. The technique can be used to explore both the complex wave field information, as well as the source-point position and its fluctuations. The latter is particularly interesting for short FEL beamlines and yields valuable information about the gain length of the source [27].

Optics EXPRESS

To assess the effectiveness of this approach, we performed a wave field characterization experiment at the FLASH facility [28], which shares many properties with the European XFEL, a hard X-ray FEL source to come online in 2017. The experiment was accompanied by simulations with a geometry identical to that used in the FLASH experiment at beamline BL2.

2. Conceptual design and theoretical considerations

The experimental setup for a focused FEL at FLASH beamline BL2 is conceptually shown in Fig. 1. In [21], Quiney *et al.*, the distance between the source and the focusing element is

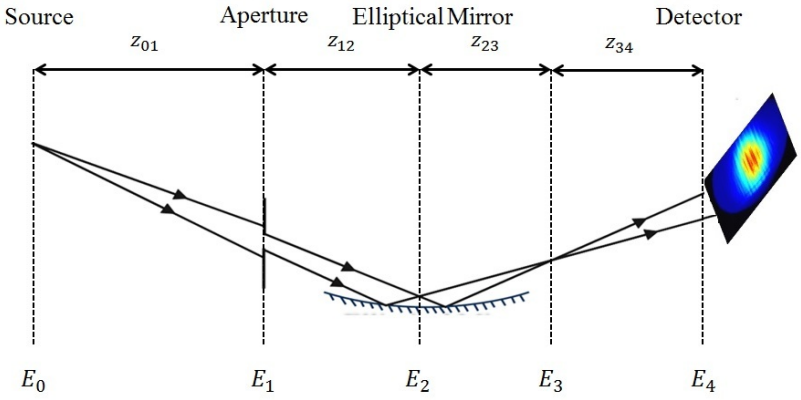

Fig. 1. The focused wave field characterization geometry. Soft x-rays of wavelength λ are clipped by a 5 mm circular aperture and focused by an elliptical mirror with 2 m nominal focal length. A two-dimensional detector (CCD) is located downstream of the focal plane where the Fresnel number satisfies the far-field condition.

assumed to be infinite. Here we account for a finite distance $z_{02} = z_{01} + z_{12}$ between the source and the elliptical mirror, so that the beam is focused at a distance z_{23} from the mirror which is slightly larger than its nominal focal length f. As a prerequisite of the IPRAs, a plane must exist along the optical axis where the wave field has a limited spatial extent in order to constrain the solution [29, 30]. For any focusing system that can be represented by a thin lens, such a constraint can be given by the finite entrance aperture of the focusing device. In [21], Quiney *et al.*, the entrance aperture of the lens is located in the same plane as the focusing element itself. Nevertheless, the support constraint can be imposed in a plane that differs from the plane of the focusing element itself [30]. Here the support-defining aperture is located at a distance z_{01} from the source, so that there is a finite propagation distance z_{12} between the aperture plane and the lens.

We consider the paraxial Fresnel propagation of a monochromatic scalar wave $\Psi(\rho_i, z_i)$ of wavelength λ [31]:

$$\Psi(\rho_j, z_j) \simeq \exp(ikz_{ij}) F^{-1} \exp(-iz_{ij}\frac{k_\perp^2}{2k})\ F\ \Psi(\rho_i, z_i)\ = \Upsilon(\Psi(\rho_j, z_j), \tag{1}$$

here $\rho_j = (x_j, y_j)$ denotes the Cartesian coordinates in a plane perpendicular to the optical axis, $z_{ij} = z_j - z_i$ is the distance between the i-th and j-th plane along the optical axis, ρ_i equals $(x_i^2 + y_i^2)^{1/2}$, k is the wave number and F represents the two-dimensional Fourier transform with respect to x and y. For simplicity, we introduced an operator notation format. Equation 1 is numerically stable for Fresnel numbers FN>> 1 [32]. For FN<< 1, the equivalent far-field

Optics EXPRESS

formulation of Fresnel propagation reads as

$$\Psi(\rho_j, z_j) \simeq -\frac{i}{\lambda z_{ij}} \exp(i\frac{k}{2z_{ij}}\rho_j^2)\, F(\exp(i\frac{k}{2z_{ij}}\rho_i^2)\,.\,\Psi(\rho_i, z_i)) \simeq \Sigma(\rho_j, z_j)\, F(\Omega(\rho_i, z_{ij})\,.\,\Psi(\rho_i, z_i)). \tag{2}$$

The experimental geometry at beamline BL2 is designed such that Eq. 1 is valid for propagation distance z_{12} whereas Eq. 2 describes propagation over distances z_{23} and z_{34}.

To recover the complex wave field in the detector plane we use an extension of the iterative algorithm presented by Quiney *et al.* [21]. More specifically, we introduce an additional propagation between the entrance aperture and the focusing element. In addition, we consider a finite distance between source and aperture plane. Consequently, we require reciprocal propagation between four planes: The support plane E_1, the elliptical-mirror plane E_2, the approximate focal plane E_3, and the detector plane E_4.

Representing the wave field $\psi(\rho_4, z_{34})$ at the detector plane as a product $\psi^d \exp(i\frac{k}{2z_{34}}\rho_4^2)$ of a (nearly) planar and spherical component, the algorithm can be described as follows:

1. $\psi(\rho_3, z_3) \simeq \Sigma(\rho_3, -z_{34})\,.F(\psi^d_{guess})$,
2. $\psi(\rho_2, z_2) \simeq \Sigma(\rho_2, \frac{z_{23}.f}{z_{23}-f})\, F(\Omega(\rho_3, -z_{23})\,.\,\psi(r_3, -z_{23}))$,
3. $\psi(\rho_1, z_1) \simeq \Upsilon^{-1}(\psi(\rho_2, -z_{23}))$,
4. Impose support constraint on $\psi(\rho_1) \rightarrow \psi_{New}(\rho_1)$,
5. $\psi(\rho_2, z_2) \simeq \Upsilon(\psi_{New}(\rho_1, z_{12}))$,
6. $\psi(\rho_3, z_3) \simeq \Sigma(\rho_3, z_{23})\, F(\Omega(\rho_2, \frac{z_{23}.f}{f-z_{23}})\,.\,\psi(\rho_2, z_{12}))$,
7. $\psi(\rho_4, z_4) \simeq \frac{-i}{\lambda z_{34}}\,.\,F(\Omega(\rho_3, z_{34})\,.\,\psi(\rho_3, z_{23}))$
8. Impose wave field amplitude constraint on $\psi(\rho_4) \rightarrow \psi_{New}(\rho_4)$,
9. Substitute $\psi_{New}(\rho_4)$ as ψ^d_{guess} in step 1.

Here f denotes the nominal focal length of the elliptical mirror and ψ^d_{guess} is a random complex wave field to initiate the algorithm.

The discrete Fourier transform (DFT) relation defines the pixel sizes between two consecutive planes and are given by:

$$\delta x_i = \delta x_j \quad (FN >> 1), \tag{3}$$

$$\delta x_i = \frac{\lambda z_{ij}}{N \delta x_i} \quad (FN << 1), \tag{4}$$

where δx_{ij} is the linear pixel size in two planes linked by the DFT, N is the pixel number in the discrete array, λ is the wavelength of x-ray and z_{ij} is the linear distance between two planes.

The Shannon sampling condition, to adequately sample quadratic terms involving in both Fresnel formalisms can be expressed as follows [33, 34]:

$$\frac{\lambda z_{ij}}{N(\delta x_i)} \leq 1 \quad (E_1 \leftrightarrow E_2), \tag{5}$$

$$\frac{\lambda z_{ij}}{N(\delta x_i)} \geq 1 \quad (E_2 \leftrightarrow E_3 \; and \; E_3 \leftrightarrow E_4) \tag{6}$$

here δx_i identifies the numerical sampling at the plane of propagation and $\leftrightarrow$ refers to a reciprocal propagation between two consecutive planes.

As the source-distance z_{01} is only approximately known, the exact distance of the image plane from the focusing mirror has to be retrieved numerically by propagating the reconstructed wave field along the optical axis in a small neighborhood around plane E_3. Here we use a sharpness metric [35],

$$S(z) = \iint I^2(x, y; z)\, d^2 r\,, \tag{7}$$

to localize the exact location of the image plane, i.e. the focus of the imaging system.

Optics EXPRESS

As shown below, the algorithm allows one to recover the complex wave field incident on the entrance aperture. The phase curvature of the recovered wave field then allows the determination of the longitudinal source-point position for each single-shot. In the first few iterations we use *a-priori* knowledge of the support and in further iterations, the shrink-wrap algorithm [19]. To this end, the intensity of a blurred version of the current estimate of the wave field, a 125 × 125 pixels Gaussian distribution with a zero mean and standard deviation of 2 pixels was used, and updated every 10 iterations, to finalise the accurate extent of the support.

The measure of the algorithm convergence, ϵ, is defined as commonly used in the single-plane CDI phase recovery [30]. For the p-th measured intensity the Fourier space reconstruction error is defined as

$$\epsilon_p = \sqrt{\frac{\sum_{ij}(|\psi^p(r_4, z_{34})| - \sqrt{I^p_{measured}})^2}{\sum_{ij} I^p_{measured}}}, \tag{8}$$

where i,j represent the detector pixel coordinates in horizontal and vertical direction, respectively. Once convergence has been achieved, i.e. the error has reached a low steady state, the algorithm is halted at step 7, which then constitutes the best estimate of the wave field distribution in the detector plane.

3. Simulation

To validate the algorithm's performance, we simulated the focus characterization experiment at FLASH beamline BL2, as shown in Fig. 1. Soft x-rays of wavelength 14.7 nm are cropped by a 5 mm circular aperture and focused by an elliptical mirror with 2 m nominal focal length. A 2D pixellated detector containing 1024×1024 pixels with a pixel pitch of 13 μm, is located downstream of the focal plane where the Fresnel number satisfies the far-field condition. In order to simulate the forward propagation of the wave field to the detector plane, we follow steps 5 to 7 of the algorithm. The distances are defined as: z_{01} = 71.5 m, z_{12} = 3.85 m, $z = z_{23} + z_{34}$ = 3.2 m.

A random, low-pass filtered intensity distribution is used as the incident intensity at the aperture plane, and the incident phase is taken to be spherical with a radius of 71.5 m. Thus, the image plane is located at 2.054 m downstream of the elliptical mirror(Fig. 2). A Gaussian noise distribution was added to the diffraction pattern with an average of zero and a standard deviation of 3% of the signal level. This was conducted to observe the algorithm's performance in the presence of an imperfect signal. For many trials of simulation, different levels of noise were considered. It was observed that, with a noise level less than 8% of the signal level, the algorithm converges to a reliable solution according to the relative difference between the reconstructed noisy and noise-free simulated wave fields,

$$Q = \frac{\sum_{ij} I^{no}_{rec} - \sum_{ij} I^{id}_{rec}}{\sum_{ij} I^{id}_{rec}} \tag{9}$$

where I^{id}_{rec} presents the reconstruction of a noise free pulse, and I^{no}_{rec} is the reconstruction of the same pulse with noise added. $\sum_{ij}$ is a summation over the discrete array.

For a small noise level (1-2%) this difference is also quite small (Q = 0.003), and the relative difference increases to a value of Q = 0.03 for a noise level of 8%.

The approximate image plane position (E_3) was chosen as z_{23} = 2.044 m for the algorithm, to be corrected at the end using the sharpness metric (Eq. 7) on the final reconstruction. 200 iterations were applied for reconstruction. The algorithm was initialized at the detector plane by a random phase varying in the range [-π,π].

Figure 3 summarizes the results from the reconstruction of the simulated input wave field at the aperture plane. A 1D-profile comparison of the simulated and reconstructed phase within the aperture indicates an accurate reconstruction with a rms error of $0.05\lambda_{14.7}$. The phase was unwrapped here using a 2D version of the 3D unwrapping algorithm described in [36]. An average pixel-wise residual of less than 1% was observed in the reconstructed intensity. As seen in Fig. 3(c), the reconstruction error monotonically approaches a minimum after 150 iterations. The support considered in the simulation was retrieved successfully within the first few iterations of the shrink-wrap algorithm. *A-priori* knowledge of the support can potentially speed up the algorithm convergence, however, the support can be reconstructed by the shrink-wrap algorithm given minimal information about the support.

Optics EXPRESS

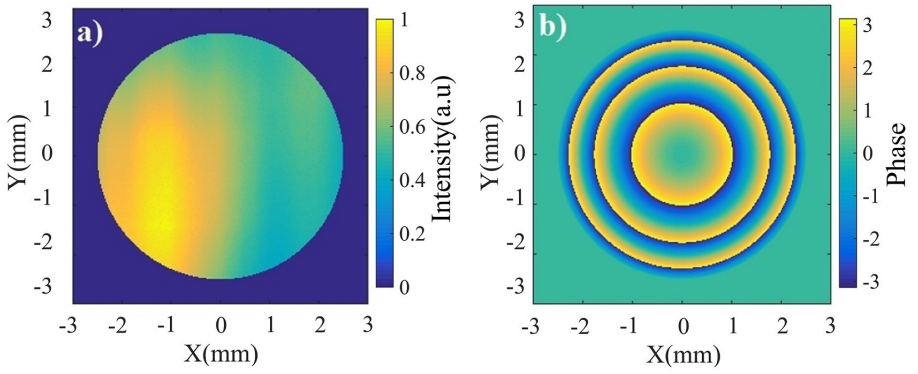

Fig. 2. Simulated divergent wave field. (a) and (b) show the input intensity and phase for a wave field illuminating the aperture. The image are 1024×1024 pixels with 23.3 μm square pixels. The source-to-aperture distance is 71.5 m and the wavelength is 14.7 nm.

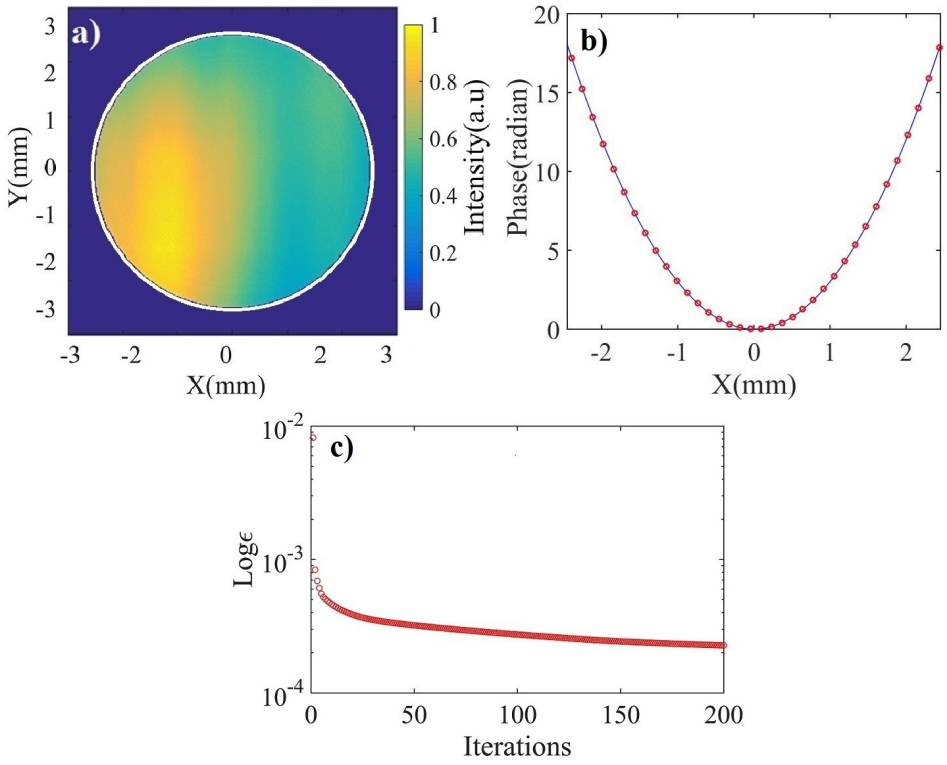

Fig. 3. Input wave field reconstruction at the aperture plane. A visual comparison of the reconstructed (a) and simulated intensity (see Fig. 2) confirms a good quantitative recovery. The white circle in (a) represents the extent of the successfully reconstructed support. (b) displays a central line profile comparison of the simulated (blue line) and reconstructed (red dots) phase concluding an accurate reconstruction. The error evaluation is depicted in (c).

After performing 50 simulated trials the average position of the image plane was obtained by back-

Optics EXPRESS

propagating the reconstructed wave field and using Eq. 7, as shown in Fig. 4(a). This yields z_{23} = 2.054 m with a standard deviation of Δz = ±2 mm, which indicates the uncertainty in source position that can be ascribed to the algorithm. A meridional profile of the simulated and reconstructed intensity at the image plane verifies the ability of the algorithm to reconstruct the localized wave field as depicted in Fig. 4(b). Further successful simulations were performed, that are not reported here for brevity.

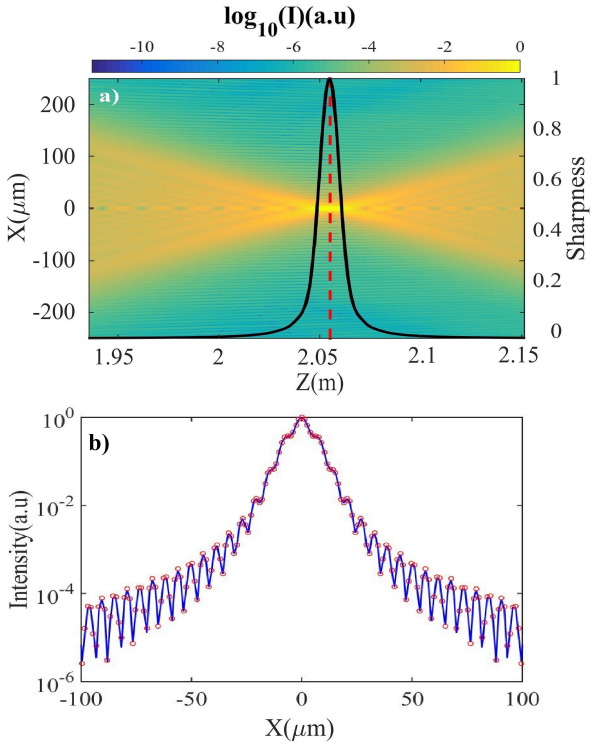

Fig. 4. The image plane wave field reconstruction of the simulated data. A meridional profile of the focused wave field's intensity is shown in (a). The image plane on-axis location (red dashed line) was determined accurately (z = 2.054 m) using Eq. (7) as plotted (black curve) in (a). In (b) the line profile of the intensity distribution for reconstructed (red dots) and simulated (blue line) wave field are depicted on a logarithmic scale to highlight the full recovery of the contribution of the sidelobes. Note that the sharpness is normalized to unity in (a).

4. Experiment and results

The experiments were performed at FLASH1 beamline BL2. The photon energy was set to 84.3 eV, corresponding to a wavelength λ = 14.7 nm with a pulse energy up to 15.2 µJ. During the experiment the beam was attenuated using niobium and zirconium filters (with a thickness of 289 nm and 1500 nm, respectively) to allow the observation of the direct beam with 2D detectors and to block the higher harmonic components from the undulators. The pulses were delivered with a weak electron bunch compression [37] using six active undulator segments to generate spatially coherent pulses [38].

The position of the approximate image plane was also chosen as identical to the simulation for each single-shot reconstruction. The data were collected by a direct-conversion CCD detector (Andor iKon-M SO DO934P-BN) with a black-illuminated chip and the same geometry as in the previous section. Dark frames were collected repeatedly during the experiment, averaged and used for background subtraction on

Optics EXPRESS

a pixel by pixel basis according to:

$$I^{corr} = \max\{I^{frame} - (1+\alpha)I^{dark}, 0\}. \quad (10)$$

α here denotes the standard deviation of the dark images, relative to its mean, which in practice is very close to zero ($\simeq 10^{-3}$).

A subset of data was selected by including frames which are correlated with a deliberately measured reference frame taken during the experiments. This enables us to disregard known instabilities in the apparatus and beamline, as well as the occasional loss of beam observed during the experiments, and observe only the meaningful variations of the source.

The reconstructions were performed by ascribing a random phase to the measured amplitudes to initiate the algorithm. The wave field reconstruction was found to be reliable and reproducible upon 20 trials for every single-shot by monitoring the lowest values of ϵ_p. A deviation of 5%, between these minimum values, was found and the absolute ϵ_p was less than 10^{-3}, indicating good convergence. The algorithm reached a steady state within 200 iterations. For a subset of data, the algorithm was run for one thousand of iterations, for each data frame, and no further improvement in convergence is observed after 200 iterations.

Figure 5(a) shows the reconstructed complex wave field of a frame Ψ_R in the image plane with the lowest value of the final error within the data set. The meriodinal intensity distribution is depicted in Fig. 5(b). An average source image size (i.e.focus size) of $9.5_{\mathrm{v}} \times 9.55_{\mathrm{h}}$ μm^2(intensity FWHM) is found by the reconstructions over the 80 pulses out of 150 pulses measured. On average, a longitudinal focus position of $\bar{z}_{23} = 2.060$ m with a standard deviation of $\Delta z = \pm 4$ mm is determined, indicating image-plane on-axis fluctuations smaller than the Rayleigh range.

The longitudinal fluctuations of the image plane reflects a source position variation along the undulator segments (Fig. 6). The average source position ($\bar{z}_{01}$) was obtained as approximately 69 m with a standard deviation of 2 m. It can be seen that the mean source position during the experiment was upstream of the end of the last undulator [39].

5. Comparison with HWS method

In addition to the diffaction measurements, the experimental setup was equipped with a removable, planar refractive Au mirror which guides the FEL beam under 90° onto a Hartmann wavefront sensor. This sensor was built by the company Imagine Optic [40]. The characteristic features of the sensor are drawn in Table 1 [12]. It operates in the wavelength region from 10 nm to 40 nm, which is within the accessible FLASH wavelength range. The Hartmann wavefront sensor was operated by the software MrBeam which was developed by the Laser-Laboratorium Göttingen e.V. [41].

Table 1. Overview of the Hartmann sensor at FLASH beamline BL2

Camera	Hartmann Plate
Princeton Instruments PI-SX: 1300 1340(H) x 1300(V) pixels 19.5 mm(H) x 19.5 mm(V) field of view	quadratic holes 110 µm x 110 µm pitch size 387 µm 250 mm plate to CCD (80 µm thick Ni plate)

When a complex wave field illuminates the the Hartmann plate (pinhole array), a set of dissected diffraction patterns is measured by the camera. The intensity and phase of the complex wave field thus can be retrieved by analyzing the diffracted spots either in real or Fourier space. Here we used the Fourier demodulation method to retrieve the complex wave field at the detector plane. The detail of this technique can be found elsewhere [42–45]. After reconstructions, the same procedure as described previously was applied to find the longitudinal position of the image plane associated with every single-shot.

In Fig. 7 the reconstructed complex wave field in the image plane of a frame which has the same longitudinal position as Ψ_R is shown. Within the data set, the average source image size is determined to be $9.6_{\mathrm{v}} \times 9.62_{\mathrm{h}}$ μm^2(Intensity FWHM). The average image plane location is obtained $\bar{z}_{23} = 2.061$ m with a standard deviation of $\Delta z = \pm 6$ mm.

Additionally, the data sets measured by the Hartmann sensor were separately analyzed using the MrBeam software [41]. Here, the complex wave field retrieval was performed in real space by resolving the

Optics EXPRESS

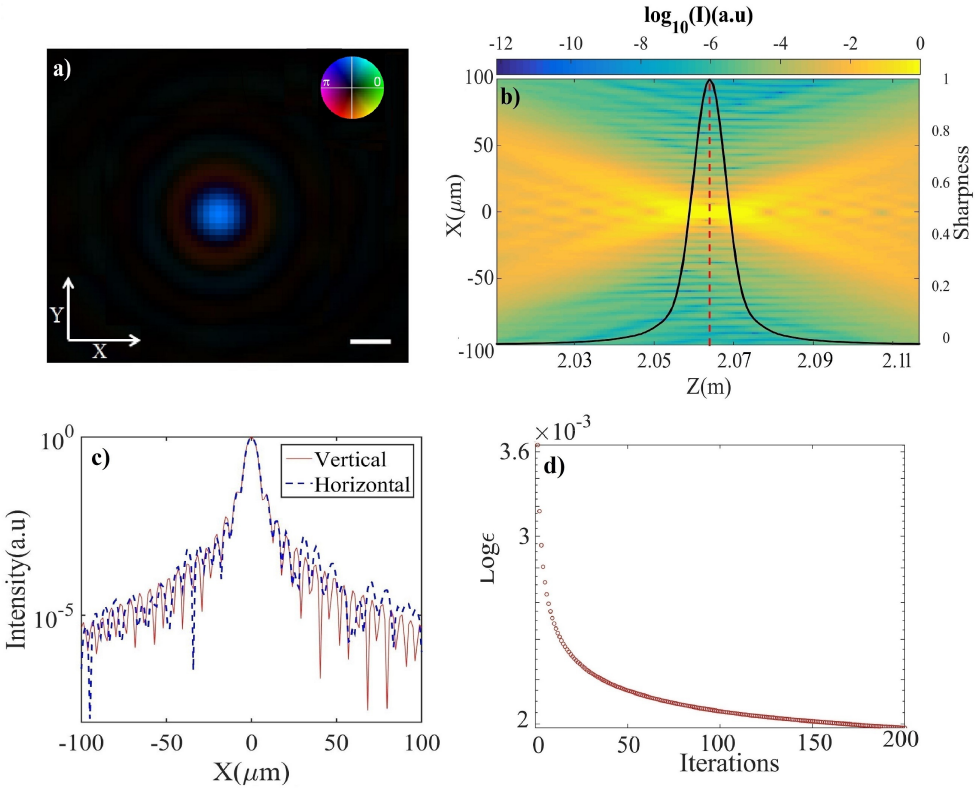

Fig. 5. The iteratively reconstructed complex wave field in the image plane of an individual FLASH pulse with the lowest level of the final error within the data set measured. In (a) phase is expressed by the hue and intensity by the brightness. (b) displays the full caustic of the pulse. The red dashed line indicates the image plane location as z_{23} = 2.064 m. (c) displays the lateral line profiles of the intensity distribution at the image plane in a logarithmic scale. The FWHM was estimated as $9.5_v \times 9.5_h$ μm^2. The algorithm convergence is shown in (d). Note that no obvious aberrations are resolved, showing the limited resolution in this particular case. The solid white line is a 20 μm scales bar.

displacement of the diffraction patterns measured against a reference pattern, previously measured at the BL2 beamline as an average over one thousand single pulses [12]. The mean focus size was found to be $11_v \times 13_h$ μm^2(Intensity FWHM) with a standard deviation of 1 μm for the both lateral directions. The result shows a slightly larger focus size compared to the demodulation method, which may be attributed to the limited spatial sampling (the pitch size of Hartmann array).

It is clearly seen that the results of the HWS method, in real and Fourier space, are in general agreement with those obtained by the iterative imaging technique, building further confidence in the validity of our iterative reconstructions.

6. Conclusion

We have demonstrated numerically and experimentally an algorithmic phase retrieval approach to characterize coherent, focused FEL pulses on a single-shot basis. The results obtained compare favorably with the established HWS method performed with the same FEL parameters. A high level of correlation was observed between the results of both methods, illustrating the ability of the new iterative method

Optics EXPRESS

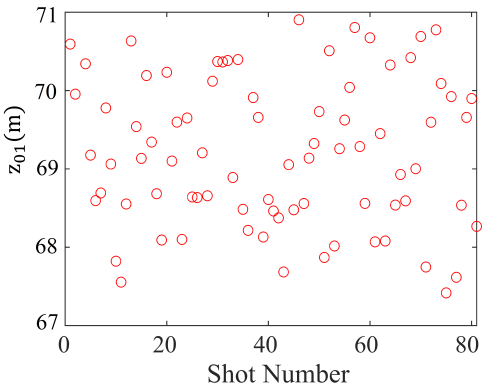

Fig. 6. Longitudinal source position fluctuation (z_{01}). The longitudinal fluctuations elucidate a gain variation along the undulator segments.

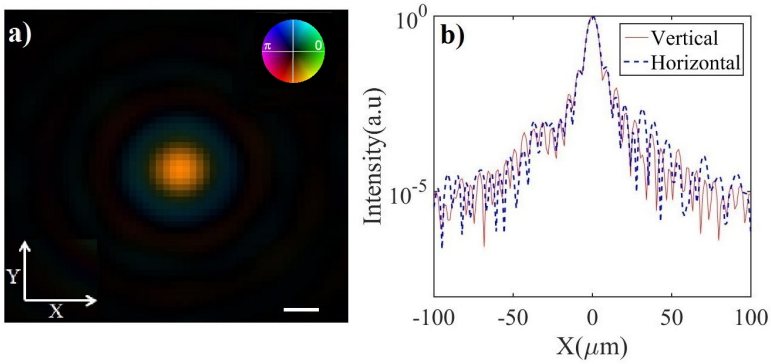

Fig. 7. The HWS reconstructed complex wave field in the image plane of a pulse having the same longitudinal position as Ψ_R. In (a) phase is expressed by the hue and intensity by the brightness. (b) displays the lateral line profiles of the intensity at the image plane. The FWHM was estimated as $9.63_v \times 9.63_h$ μm^2. The solid white line is a 20 μm scales bar.

to reconstruct focused wave fields without the need for using conventional manipulative optics such as absorbing screens.

It should be noted that the comparison between both HWS and iterative methods was made due to the applicable FEL energy of FLASH for the Hartmann sensor. In general, Hartmann plates function well for softer energy ranges and may not apply to the hard photon energies at XFELs, such as the European XFEL. The iterative imaging method—not relying on the properties of absorptive optics between the focusing optics and detector—provides a general technique applicable across a very broad photon energy range, as well as for different focusing optics. Elsewhere we have shown explicitly through simulation the applicability of this method at hard X-ray energies, specifically for the upcoming SPB/SFX instrument of the European XFEL [46].

As the exact on-axis position of the image plane for every single-shot is resolved, the associated longitudinal source-position fluctuations can be found. This enables, for example, monitoring of the source gain variation within the active undulators of an FEL source.

Optics EXPRESS

Funding

Deutsche Forschungsgemeinschaft (DFG EXC 1074).

Acknowledgments

We thank K.A. Nugent, G.J. Williams, T. Tschentscher and H. N. Chapman for many stimulating discussions, as well as L. Mikeš for helpful suggestions in the numerical simulations. This work has been supported by the excellence cluster 'The Hamburg Centre for Ultrafast Imaging - Structure, Dynamics and Control of Matter at the Atomic Scale'.